

Complete NLO QCD Corrections to ZZ Production in Gluon Fusion

Bakul Agarwal,^{1,2,*} Stephen Jones,^{3,†} Matthias Kerner,^{1,‡} and Andreas von Manteuffel^{4,2,§}

¹*Institute for Theoretical Physics, Karlsruhe Institute of Technology (KIT), D-76131 Karlsruhe, Germany*

²*Department of Physics and Astronomy, Michigan State University, East Lansing, Michigan 48824, USA*

³*Institute for Particle Physics Phenomenology, Durham University, Durham DH1 3LE, UK*

⁴*Institut für Theoretische Physik, Universität Regensburg, 93040 Regensburg, Germany*

We calculate the complete NLO QCD corrections to loop-induced $gg \rightarrow ZZ$ production including full top-quark mass effects. The two-loop virtual corrections are obtained by combining analytic results for the massless, Higgs-mediated, and one-loop factorizable contributions with numerically computed amplitudes containing the top-quark mass. We show that the choice of subtraction scheme for the virtual contribution impacts the precision with which the virtual contribution must be evaluated in order to obtain sufficiently precise phenomenological predictions. For direct production through a massive top-quark loop, we observe that the relative NLO corrections are large. The direct massive and Higgs-mediated contributions individually increase relative to the massless production at high diboson invariant mass, but interfere destructively with each other. At the Large Hadron Collider, the NLO corrections to the gluon channel give a sizable contribution to the $pp \rightarrow ZZ + X$ cross-section at N³LO.

INTRODUCTION

The advent of the High-Luminosity LHC brings exciting opportunities to measure Standard Model parameters at unprecedented precision. An important process in this regard is the production of a pair of Z bosons, which is relevant for new physics searches [1–4] and provides a significant background to Higgs production in the four-lepton channel [5–8], both for on- and off-shell Higgs bosons. Z boson pair production has been measured at 13.6 TeV [9] and used to constrain anomalous CP-odd neutral triple gauge couplings [10]. Comparing resonant and non-resonant Higgs production allows for an indirect probe of the Higgs width [11, 12], and continuum Z pair production can contribute significantly to off-shell Higgs production through interference [13, 14]. Constraints on the Higgs width have been obtained in this way both by the CMS [15] and ATLAS experiments [16]. Given the phenomenological relevance, precise theoretical predictions for the Z pair production process are desirable.

The gluon fusion channel for Z pair production is loop induced and starts to contribute to the hadronic process $pp \rightarrow ZZ + X$ only at next-to-next-to-leading order (NNLO). Owing to high gluon luminosity at the LHC, this channel accounts for O(60%) of the total NNLO correction to the process [17]. NLO corrections to this channel are formally next-to-next-to-next-to-leading order (N³LO) with respect to the hadronic process. In general, different partonic channels mix at higher orders in the perturbative expansion such that the concept of corrections to a specific subprocess is not well defined. In the present case, however, one can define NLO corrections to the gluon channel by considering only the contributions in which neither of the Z bosons couples to external quark lines. The so-defined NLO corrections are indeed significant: estimates using only massless quarks [18] or including an approximate massive contribution [19] give

an overall O(5-8%) increase to the total $pp \rightarrow ZZ$ cross-section. For the two-loop amplitudes, the massless corrections were computed a while back in [20, 21], while the top-quark contributions remained a challenge until recently, preventing the calculation of the exact NLO QCD corrections in this channel so far. The top-quark contributions are known to be important, particularly in the high invariant mass region for the production of longitudinal Z bosons due to the Goldstone boson equivalence theorem [22, 23] and the interplay with Higgs-mediated production. Approximate NLO corrections to $gg \rightarrow ZZ$ have been presented in [24–28] and supplemented with a parton shower in [29, 30]. Recently, the two-loop amplitudes have been calculated with full top-quark mass effects [31, 32].

In this letter, we take the next step and calculate the complete NLO QCD corrections to $gg \rightarrow ZZ$ with full top-quark mass effects. Specifically, we consider all contributions to the cross-section involving closed massless or massive quark loops to which the external Z bosons couple either directly or through a Higgs boson. For the real radiation contributions, we take into account also gq , $g\bar{q}$ and $q\bar{q}$ in addition to gg initial states. Using a fully differential setup, we compute the inclusive cross-section and the diboson invariant mass distribution for ZZ production at the LHC.

DETAILS OF THE CALCULATION

The differential cross-section for $gg \rightarrow ZZ$ at NLO accuracy can be written as

$$d\sigma_{\text{NLO}} = d\sigma_{\text{B}} + d\sigma_{\text{V}} + d\sigma_{\text{R}}, \quad (1)$$

where $d\sigma_{\text{B}}$, $d\sigma_{\text{V}}$, and $d\sigma_{\text{R}}$ correspond to Born, virtual, and real contributions, respectively. In our calculation, we include effects due to $n_f = 5$ massless quark flavors, a

massive top-quark, and a massive Higgs boson. The calculation of the different contributions is described below.

Born and virtual contributions

We consider the partonic process

$$g(p_1) + g(p_2) \rightarrow Z(p_3) + Z(p_4), \quad (2)$$

with momenta p_1 and p_2 incoming and p_3 and p_4 outgoing such that $p_1 + p_2 = p_3 + p_4$. The external particles are taken on-shell, i.e.

$$p_1^2 = p_2^2 = 0, \quad p_3^2 = p_4^2 = m_Z^2, \quad (3)$$

and the Mandelstam variables are defined as

$$\hat{s} = (p_1 + p_2)^2, \quad \hat{t} = (p_1 - p_3)^2, \quad \hat{u} = (p_2 - p_3)^2, \quad (4)$$

with $\hat{s} + \hat{t} + \hat{u} = 2m_Z^2$. The amplitude for this process can be written as

$$\mathcal{M}_\lambda^{ab} = \mathcal{M}_{\mu\nu\rho\sigma} \epsilon_1^\mu \epsilon_2^\nu \epsilon_3^\rho \epsilon_4^\sigma \delta^{ab}, \quad (5)$$

where $\lambda = \{\lambda_1, \lambda_2, \lambda_3, \lambda_4\}$ specify the polarizations of the external particles and $\epsilon_i = \epsilon_{\lambda_i}(p_i)$. The color indices a, b of the two gluons will be suppressed in the following. The tensor amplitude can be decomposed into 20 form factors [20] according to

$$\mathcal{M}^{\mu\nu\rho\sigma} = \sum_{i=1}^{20} A_i(\hat{s}, \hat{t}, m_Z^2, m_q^2) T_i^{\mu\nu\rho\sigma}. \quad (6)$$

We can define helicity amplitudes for a specific choice of polarizations in the partonic center-of-momentum frame. Explicit definitions of helicity amplitudes in terms of the form factors in (6) are provided in the ancillary files of [31].

The one-loop amplitudes relevant for the Born contribution have been calculated long ago in Refs. [33–35], while the two-loop corrections employed for this paper were completed only more recently. We distinguish between different classes of contributions to the amplitude, depending on the couplings of the external Z bosons. Figure 1 shows a representative two-loop Feynman diagram for each of the following classes.

Class A_h: Both Z bosons couple directly to the same heavy top-quark loop. For these one- and two-loop contributions, we use the recent calculation [31] by some of us for which a combination of syzygy techniques [31, 36–40], finite field methods [41, 42], multivariate partial fractioning [43–47], and constructions of finite integrals were employed, and the resulting finite master integrals were evaluated numerically with `pySecDec` [48–50].

Class A_l: Both Z bosons couple directly to the same light quark loop. Analytical expressions for these one-

and two-loop contributions with zero quark mass were provided in [20], based on solutions for the master integrals [51] in terms of multiple polylogarithms. We employ their implementation in the `VVamp` library and numerically evaluate the multiple polylogarithms using the code of Ref. [52] included in `GiNaC` [53].

Class B: The Z bosons couple to different closed quark loops, each of which can be a light or a heavy quark. At two loops, these corrections are one-particle reducible products of one-loop triangles. Among all two-loop corrections, it is only these diagrams for which Dirac traces with an odd number of γ_5 matrices need to be considered and contributions related to the chiral anomaly can arise due to a mass splitting within a weak iso-doublet. Consequently, one should consider them for sums over a complete quark generation, and for our calculation with five massless quarks just the third generation contributes due to $m_b \neq m_t$. These contributions have been presented in [26]; we use the recalculation in [31] for this work.

Class C: The Z -boson pair is produced via the decay of an intermediate off-shell Higgs boson, which couples to a heavy quark loop. We employ an in-house implementation of these Higgs-mediated contributions based on the differential equations approach, similar to the calculation in [54]. In the high invariant mass region, above the top-quark threshold, one finds interesting interferences between the Higgs-mediated and direct production of longitudinally polarised Z bosons. At one-loop, it has been discussed in [34] that the interference is destructive and exhibits a cancellation of the leading term at high energy, as required by the unitarity of the $t\bar{t} \rightarrow ZZ$ subprocess; we observe a strong destructive interference also at two-loops.

After UV renormalization and IR subtraction, details of which are provided in Refs. [20, 31], the finite remainders for the helicity amplitudes can be written as

$$\mathcal{M}_\lambda^{\text{fin}} = \left(\frac{\alpha_s}{2\pi}\right) \mathcal{M}_\lambda^{(1)} + \left(\frac{\alpha_s}{2\pi}\right)^2 \mathcal{M}_\lambda^{(2)} + \mathcal{O}(\alpha_s^3), \quad (7)$$

where $\mathcal{M}_\lambda^{(1)}, \mathcal{M}_\lambda^{(2)}$ are the one- and two-loop finite remainders. We define squared one-loop amplitudes $\mathcal{V}^{(1)}$ as well as the interference between one- and two-loop amplitudes $\mathcal{V}^{(2)}$ as

$$\mathcal{V}^{(1)} = \frac{1}{N} \sum_{\lambda, \text{color}} \mathcal{M}_\lambda^{*(1)} \mathcal{M}_\lambda^{(1)}, \quad (8)$$

$$\mathcal{V}^{(2)} = \frac{1}{N} \sum_{\lambda, \text{color}} 2 \text{Re} \left(\mathcal{M}_\lambda^{*(1)} \mathcal{M}_\lambda^{(2)} \right), \quad (9)$$

where we divide by $N = 2^2 \cdot 8^2 \cdot 2$ to account for the averaging over spins and colors in the initial state and the symmetry factor due to identical particles in the final state.

To optimize the sampling of the virtual amplitude for our full result, we separate the amplitude according to

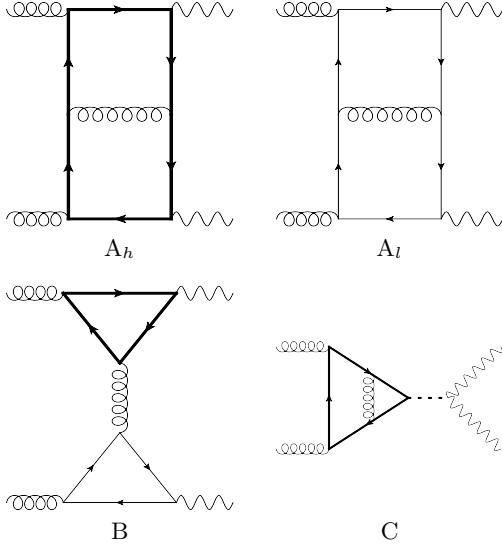


Figure 1: Representative two-loop diagrams with closed quark loops entering the virtual corrections to ZZ production. Thick lines denote top quarks.

the masses of the intermediate particles,

$$\mathcal{M}_\lambda^{(2)} = \mathcal{M}_{\lambda,A_h}^{(2)} + \mathcal{M}_{\lambda,A_l}^{(2)} + \mathcal{M}_{\lambda,B}^{(2)} + \mathcal{M}_{\lambda,C}^{(2)}, \quad (10)$$

where the subscript denotes the class of contributing diagrams as defined above. Inserting the decomposed two-loop virtual amplitude into Eq. 9, the interference with the full Born amplitude $\mathcal{M}^{(1)}$ can be written as

$$\mathcal{V}^{(2)} = \frac{1}{N} \sum_{\lambda, \text{color}} 2 \text{Re} \left(\mathcal{M}_\lambda^{*(1)} \mathcal{M}_{\lambda,A_h}^{(2)} + \mathcal{M}_\lambda^{*(1)} (\mathcal{M}_{\lambda,A_l}^{(2)} + \mathcal{M}_{\lambda,B}^{(2)} + \mathcal{M}_{\lambda,C}^{(2)}) \right). \quad (11)$$

We sample the first interference term using massive virtual amplitude evaluations distributed according to unweighted events based on the top-quark only Born distribution, as described below. The remaining Born-virtual interference terms are evaluated with higher statistics: they are sampled dynamically by our phase-space generator code using the VEGAS algorithm [55, 56], with an additional weight to ensure that sufficiently many events are generated at high invariant mass.

By default, we use the q_T subtraction scheme [57] for our two-loop amplitudes and the Catani-Seymour scheme [58] to construct the dipoles for our real radiation diagrams. This mismatch amounts to a term proportional to the Born contribution which is straightforward to add/subtract from the virtual/real contributions as we desire. Similarly, we can obtain the virtual and real contributions in the original Catani subtraction scheme [59] by adding terms proportional to the Born contribution. Starting with the I-operator in the q_T scheme, we can obtain results in the Catani and Catani-Seymour sub-

traction schemes by adding $2\text{Re}(\Delta\mathbf{I}) \cdot \mathcal{V}^{(1)}$ to $\mathcal{V}^{(2)}$, where

$$\Delta\mathbf{I}_C = -\frac{1}{2}\pi^2 C_A + i\pi\beta_0, \quad (12)$$

$$\Delta\mathbf{I}_{\text{CS}} = -i\pi C_A \left(\frac{1}{\epsilon} + \ln \left(\frac{\mu_R^2}{s} \right) \right) - \frac{\pi^2 C_A}{3} + \beta_0 + k_g, \quad (13)$$

with $\beta_0 = (11/6)C_A - (2/3)T_F n_f$ and $k_g = (67/18 - \pi^2/6)C_A - (10/9)T_F n_f$. The imaginary parts of the shifts do not contribute when computing the Born-virtual interference.

We utilise these conversions to construct our virtual and real contributions in all three schemes (q_T , Catani-Seymour, and Catani). We find that the size of the virtual contribution differs by more than an order of magnitude between the various schemes, as does the real radiation (or, more specifically, the subtraction terms) such that the total NLO result we obtain in any scheme is identical. This fact can be exploited to reduce the number of samples required for the computationally expensive virtual contribution, by selecting a scheme in which the virtual contribution is small and a larger relative error on this contribution can be tolerated. For the process at hand, we have good control of all virtual contributions and can produce precise results in any subtraction scheme; however, for other particularly challenging processes, the scheme choice of the virtual contribution offers another avenue for optimization.

The Born and virtual partonic cross-sections can be written as

$$\hat{\sigma}_i = \int d\Pi_2 \frac{1}{2\hat{s}} \mathcal{V}^{(i)}, \quad i = 1, 2, \quad (14)$$

where $\mathcal{V}^{(i)}$ is the spin and color-averaged and summed interference defined above, $1/(2\hat{s})$ is the flux factor, and $d\Pi_2$ is the 2-body Lorentz-invariant phase space. The partonic cross-section then needs to be convoluted with the parton distribution functions to produce the total hadronic cross-section

$$\sigma_i = \int dx_1 dx_2 \hat{\sigma}_i f_1(x_1, \mu_F) f_2(x_2, \mu_F), \quad (15)$$

where $f_i(x_i, \mu_F)$ are the parton distribution functions and μ_F is the factorization scale.

The original calculation of our class A_h massive virtual amplitudes was described in Ref. [31]. For the current work, we have evaluated the amplitudes at 3000 additional phase-space points. The samples were obtained on multiple GPUs using the distributed evaluation (`disteval`) feature of `pySecDec`. Our new virtual amplitude code is checked against our original code and an independent calculation using different methods described in Ref. [32].

Real contributions

The real corrections for this process include the partonic channels $gg \rightarrow ZZ + g$, $q(\bar{q})g \rightarrow ZZ + q(\bar{q})$, and $q\bar{q} \rightarrow ZZ + g$. Representative Feynman diagrams are shown in figure 2. For the real radiation diagrams, we require that both Z bosons are coupled to the closed fermion loop, in particular, we exclude diagrams that involve a Z boson coupling to an incoming or outgoing quark line.

The amplitudes for the real radiation diagrams are generated using **GoSam** [60, 61] and validated numerically at the level of individual phase-space points against **MadGraph** [62, 63] and **OpenLoops** [64] (which uses **COLLIER** [65], **CutTools** [66], and **OneLOop** [67]). To obtain stable numerical results we use the Ninja integrand reduction package [68, 69] with a quadruple precision rescue system. Our rescue system employs a three-step procedure: each point is evaluated twice in double precision after an azimuthal rotation about the beam axis; if the double results do not agree to 11 digits then the amplitude is reevaluated in quadruple precision, if the quadruple evaluation does not agree with the double results within 8 digits then a second rotated quadruple result is obtained. The result is discarded if the two quadruple results do not agree within 11 digits. With the dipole subtraction implemented as described below, we observe that almost no points are rejected.

Soft and collinear singularities arising from the phase-space integration are cancelled locally by Catani-Seymour dipoles. We apply technical cuts of $p_{T,3}/\sqrt{s} > 10^{-6}$ in our $2 \rightarrow 2$ phase-space and $p_1 \cdot p_5/\hat{s} > 10^{-14}$, $p_2 \cdot p_5/\hat{s} > 10^{-14}$ in our $2 \rightarrow 3$ phase-space, where p_5 is the momentum of the additional jet.

To obtain the Catani-Seymour dipole contributions, we compute the required spin-correlated Born matrix elements using the massless quark amplitudes from the **VVamp** library [20] and an in-house implementation of the one-loop massive quark amplitudes using **LoopTools** [70, 71] to evaluate the one-loop master integrals. For the calculation of the dipoles, we observed that the spin-correlated Born matrix elements were numerically unstable in highly soft or collinear regions. Switching to the orthogonal form factors defined in [28] improved numerical stability, and better cancellation (up to 6 digits in the production runs) in the singular regions was observed.

Our integrated real matrix elements are validated against **MadGraph** and **OpenLoops** by computing the LO ZZ plus jet cross-section with several different values of $p_{T,j}$ cut.

RESULTS

In this section, we present our NLO results for ZZ production in the gluon channel for the LHC. We set $G_F =$

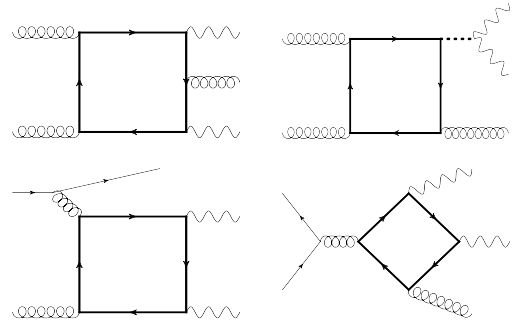


Figure 2: Representative diagrams with a closed quark loop entering the real corrections to ZZ production. Different partonic channels and loops with light or top quarks contribute.

$1.1663787 \cdot 10^{-5} \text{ GeV}^{-2}$, $m_Z = 91.1874 \text{ GeV}$, $m_W = 80.2959 \text{ GeV}$, and $m_t = 173.016 \text{ GeV}$. For the calculation of the two-loop massive amplitudes, we fix the ratio $m_Z^2/m_t^2 = 5/18$ as described in [31]. We set $\mu_R = \mu_f = m_{ZZ}/2$ as central values for renormalization and factorization scales respectively, and use the CT18NLO [72] parton distribution functions interfaced via LHAPDF [73] to calculate the total cross-section. Uncertainty estimates are obtained by simultaneously varying the renormalization and factorization scales by a factor of 2 around the central scale $\mu = m_{ZZ}/2$.

In figure 3, we show the invariant mass distribution for this process considering only diagrams of class A_h , i.e. we select one- and two-loop contributions to the amplitude for which both Z bosons couple to the same closed massive top-quark loop. The shaded bands indicate the scale uncertainty. We find that the massive NLO corrections are large, enhancing the top-only cross section by a factor of 1.8 at $\sqrt{s} = 13 \text{ TeV}$ hadronic center-of-mass energy. The NLO corrections to the Z -boson invariant mass distribution are large but rather flat; they amount to a factor 2 increase in the distribution near the ZZ production threshold and decrease to a factor of around 1.7 at 1 TeV. For the corresponding integrated cross-section at $\sqrt{s} = 13 \text{ TeV}$ we obtain, $\sigma_{\text{LO}}^{A_h} = 19.00^{+29.4\%}_{-21.4\%} \text{ fb}$, $\sigma_{\text{NLO}}^{A_h} = 34.46(6)^{+16.4\%}_{-14.4\%} \text{ fb}$, where the number in parenthesis indicates the statistical Monte-Carlo error.

In figure 3, we also show the subtracted virtual contribution obtained using different IR subtraction schemes. The NLO result does not depend on the choice of subtraction scheme, with the different schemes amounting to reshuffling contributions proportional to $\mathcal{V}^{(1)}$ between the subtracted real and virtual contributions. However, we do observe that while the virtuals in the q_T and Catani-Seymour schemes behave rather similarly, they are heavily suppressed in Catani scheme. This means that in the Catani scheme the majority of the NLO correction comes from the IR subtracted real contribution and the subtracted virtual contribution accounts for less than 2% of the total cross-section. We point out that the finite re-

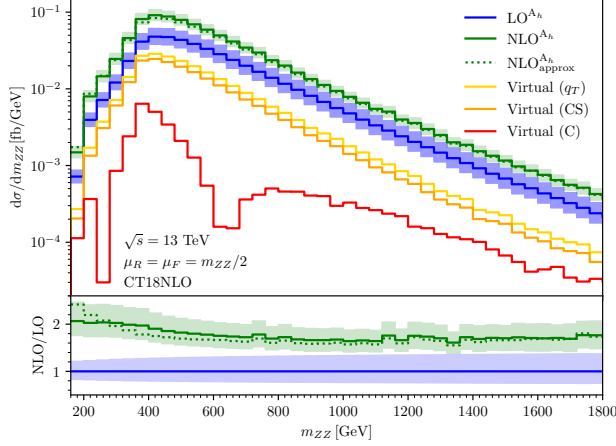


Figure 3: Top-quark-only contributions to the ZZ invariant mass distribution in pp collisions. The absolute value of the two-loop virtual correction is shown separately in the q_T , Catani-Seymour (CS), and Catani (C) schemes. The dashed curve represents an approximate NLO result obtained by rescaling the massive Born amplitude with the massless K -factor.

mainders in the Catani scheme were previously shown to be more sensitive to kinematic expansions of the two-loop expressions than in the q_T scheme [31], and may thus be interpreted as representing more directly the genuine two-loop effects. Choosing a scheme for which the virtual contributions are numerically small can be of practical importance in situations where their exact evaluation is possible but computationally expensive, since one can reduce the number of phase-space points for the numerical integration in this way. Nevertheless, in the present work, we were able to obtain sufficient statistics that the virtual could be reliably obtained in each subtraction scheme, as shown.

We also compare our results to an approximation, NLO_{approx}^{Ah} similar to [19], obtained using exact ingredients except for the massive two-loop virtual amplitudes. In this approximation, the massive two-loop virtual amplitude is replaced by the top-quark only Born amplitude rescaled by the ratio $\frac{1}{2}\mathcal{V}^{(2)}/\mathcal{V}^{(1)}$ computed using only the massless quark amplitudes. This rescaling is performed fully differentially at the level of individual phase-space points. We find that the approximation describes the exact results well in most of the phase-space for the unpolarized distributions, particularly in the high energy region.

In figure 4, we show the invariant mass distribution for ZZ production in the gluon channel for the LHC with $\sqrt{s} = 13.6$ TeV, taking into account all massless and massive contributions, including those mediated by a Higgs boson. As above, the shaded bands indicate the scale uncertainty. We find that the complete NLO correc-

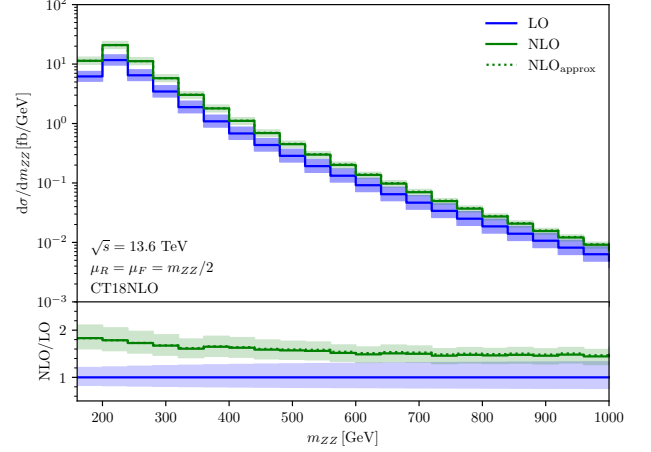


Figure 4: Diboson invariant mass distribution for gluon-initiated ZZ production at the LHC. The solid curves represent the LO and NLO results with complete massless and massive contributions, including Higgs-mediated diagrams. The dashed curve represents an approximate NLO result obtained as described in the text.

tions are large, ranging from 1.8 near the ZZ production threshold and dropping to around 1.4 at 1 TeV invariant mass.

For the dashed curve, NLO_{approx} , we again employ the approximation in which the two-loop massive virtual amplitude is replaced by the rescaled top-quark only Born amplitude, as described above. At low invariant mass, the cross-section is dominated by diagrams containing loops of massless quarks and, to a lesser extent, their interference with the Higgs-mediated contribution, both of which are included exactly in the approximation. Conversely, at high invariant mass, where the massive contribution is more important, the massive amplitudes are approximated well. As a result, we observe that the approximation works well across the entire invariant mass range for the full unpolarized NLO correction.

For the full NLO cross-section in the gluon channel at $\sqrt{s} = 13.6$ TeV with exact dependence on the top-quark mass, we obtain

$$\sigma_{LO} = 1316_{-18.0\%}^{+23.0\%} \text{ fb}, \quad (16)$$

$$\sigma_{NLO} = 2275(12)_{-12.0\%}^{+14.0\%} \text{ fb}. \quad (17)$$

Here, the number in parenthesis indicates the statistical Monte-Carlo error, while the percentages specify the uncertainty stemming from simultaneous variation of the renormalization and factorization scales by a factor of 2. The complete NLO corrections to the gluon channel are large, increasing the contribution by a factor of 1.7 compared to the leading order and beyond the naive scale uncertainty estimate. The corrections approximately half the scale uncertainty. The impact of including the direct

massive and Higgs-mediated contributions at the level of the total cross-section is moderate, decreasing the NLO cross-section by around 2% compared to purely massless contributions.

CONCLUSIONS

We have presented a complete calculation of the NLO QCD corrections to $gg \rightarrow ZZ$ retaining full top-quark-mass effects. For the LHC at center-of-mass energy $\sqrt{s} = 13.6$ TeV, we find that the total cross-section of the gluon-induced channel is enhanced by a factor of 1.7 relative to the LO correction. The diboson invariant mass distribution K-factor falls from around 1.8 at production threshold to 1.4 at 1 TeV.

We show that the choice of infrared subtraction scheme has a great impact on the accuracy with which the two-loop finite remainders need to be known. In particular, we find that in Catani's original subtraction scheme, the virtual contributions are numerically suppressed. This observation can help to reduce the computational cost for sampling these challenging contributions and should be taken into account when quantifying the quality of approximations for the finite remainders.

Our analysis shows that an approximation of the two-loop massive amplitudes by the one-loop amplitude rescaled with the massless K-factor similar to [19] is a good approximation at the level of the full unpolarized NLO invariant mass distribution.

In the future, it would be interesting to study the impact of top-quark mass effects on other differential observables and in the presence of anomalous couplings, e.g. $Zt\bar{t}$ [74, 75]. We observe that at high invariant mass there is a strong destructive interference at LO as well as NLO between diagrams in which the Z -bosons couple directly to a massive quark line and those in which the Z -bosons are produced via an intermediate Higgs-boson; this cancellation could be spoiled by such anomalous couplings. The corrections presented here contribute at N³LO to the hadronic cross-section, and should be combined with the quark-initiated contributions at least to NNLO for such phenomenological applications.

Acknowledgments We would like to thank Gudrun Heinrich, Stephan Jahn, and C.-P. Yuan for useful discussions and related work. This research was supported by the Deutsche Forschungsgemeinschaft (DFG, German Research Foundation) through grant 396021762 - TRR 257, the National Science Foundation through grant 2013859, the Royal Society through the University Research Fellowship grant URF/R1/201268, and the UK Science and Technology Facilities Council through grant ST/X000745/1. We gratefully acknowledge support and resources provided by the the High Performance Computing Center (HPCC) at Michigan State University. Our

Feynman diagrams were generated using JaxoDraw [76], based on AxoDraw [77].

* Electronic address: bakul.agarwal@kit.edu

† Electronic address: stephen.jones@durham.ac.uk

‡ Electronic address: matthias.kerner@kit.edu

§ Electronic address: manteuffel@ur.de

- [1] **ATLAS** Collaboration, G. Aad et al., *Search for heavy resonances decaying into a pair of Z bosons in the $\ell^+\ell^-\ell'^+\ell'^-$ and $\ell^+\ell^-\nu\bar{\nu}$ final states using 139 fb⁻¹ of proton-proton collisions at $\sqrt{s} = 13$ TeV with the ATLAS detector*, *Eur. Phys. J. C* **81** (2021), no. 4 332, [[arXiv:2009.14791](#)].
- [2] **ATLAS** Collaboration, G. Aad et al., *Search for heavy diboson resonances in semileptonic final states in pp collisions at $\sqrt{s} = 13$ TeV with the ATLAS detector*, *Eur. Phys. J. C* **80** (2020), no. 12 1165, [[arXiv:2004.14636](#)].
- [3] **CMS** Collaboration, A. Tumasyan et al., *Search for heavy resonances decaying to $Z(\nu\bar{\nu})V(q\bar{q}')$ in proton-proton collisions at $\sqrt{s} = 13$ TeV*, *Phys. Rev. D* **106** (2022), no. 1 012004, [[arXiv:2109.08268](#)].
- [4] **CMS** Collaboration, A. M. Sirunyan et al., *A multi-dimensional search for new heavy resonances decaying to boosted WW , WZ , or ZZ boson pairs in the dijet final state at 13 TeV*, *Eur. Phys. J. C* **80** (2020), no. 3 237, [[arXiv:1906.05977](#)].
- [5] **ATLAS** Collaboration, M. Aaboud et al., *Constraints on off-shell Higgs boson production and the Higgs boson total width in $ZZ \rightarrow 4\ell$ and $ZZ \rightarrow 2\ell 2\nu$ final states with the ATLAS detector*, *Phys. Lett. B* **786** (2018) 223–244, [[arXiv:1808.01191](#)].
- [6] **CMS** Collaboration, A. M. Sirunyan et al., *Measurement and interpretation of differential cross sections for Higgs boson production at $\sqrt{s} = 13$ TeV*, *Phys. Lett. B* **792** (2019) 369–396, [[arXiv:1812.06504](#)].
- [7] **CMS** Collaboration, A. M. Sirunyan et al., *Measurements of the Higgs boson width and anomalous HVV couplings from on-shell and off-shell production in the four-lepton final state*, *Phys. Rev. D* **99** (2019), no. 11 112003, [[arXiv:1901.00174](#)].
- [8] **ATLAS** Collaboration, G. Aad et al., *Measurements of the Higgs boson inclusive and differential fiducial cross sections in the 4ℓ decay channel at $\sqrt{s} = 13$ TeV*, *Eur. Phys. J. C* **80** (2020), no. 10 942, [[arXiv:2004.03969](#)].
- [9] **ATLAS** Collaboration, G. Aad et al., *Measurement of ZZ production cross-sections in the four-lepton final state in pp collisions at $\sqrt{s} = 13.6$ TeV with the ATLAS experiment*, [[arXiv:2311.09715](#)].
- [10] **ATLAS** Collaboration, G. Aad et al., *Evidence of pair production of longitudinally polarised vector bosons and study of CP properties in $ZZ \rightarrow 4\ell$ events with the ATLAS detector at $\sqrt{s} = 13$ TeV*, [[arXiv:2310.04350](#)].
- [11] F. Caola and K. Melnikov, *Constraining the Higgs boson width with ZZ production at the LHC*, *Phys. Rev. D* **88** (2013) 054024, [[arXiv:1307.4935](#)].
- [12] J. M. Campbell, R. K. Ellis, and C. Williams, *Bounding the Higgs Width at the LHC Using Full Analytic Results for $gg \rightarrow e^-e^+\mu^-\mu^+$* , *JHEP* **04** (2014) 060, [[arXiv:1311.3589](#)].

- [13] N. Kauer and G. Passarino, *Inadequacy of zero-width approximation for a light Higgs boson signal*, *JHEP* **08** (2012) 116, [[arXiv:1206.4803](#)].
- [14] N. Kauer, *Interference effects for $H \rightarrow WW/ZZ \rightarrow \ell\bar{\nu}_\ell\ell\nu_\ell$ searches in gluon fusion at the LHC*, *JHEP* **12** (2013) 082, [[arXiv:1310.7011](#)].
- [15] CMS Collaboration, A. Tumasyan et al., *Measurement of the Higgs boson width and evidence of its off-shell contributions to ZZ production*, *Nature Phys.* **18** (2022), no. 11 1329–1334, [[arXiv:2202.06923](#)].
- [16] ATLAS Collaboration, G. Aad et al., *Evidence of off-shell Higgs boson production from ZZ leptonic decay channels and constraints on its total width with the ATLAS detector*, *Phys. Lett. B* **846** (2023) 138223, [[arXiv:2304.01532](#)].
- [17] F. Cascioli, T. Gehrmann, M. Grazzini, S. Kallweit, P. Maierhöfer, A. von Manteuffel, S. Pozzorini, D. Rathlev, L. Tancredi, and E. Weihs, *ZZ production at hadron colliders in NNLO QCD*, *Phys. Lett. B* **735** (2014) 311–313, [[arXiv:1405.2219](#)].
- [18] F. Caola, K. Melnikov, R. Rötsch, and L. Tancredi, *QCD corrections to ZZ production in gluon fusion at the LHC*, *Phys. Rev. D* **92** (2015), no. 9 094028, [[arXiv:1509.06734](#)].
- [19] M. Grazzini, S. Kallweit, M. Wiesemann, and J. Y. Yook, *ZZ production at the LHC: NLO QCD corrections to the loop-induced gluon fusion channel*, *JHEP* **03** (2019) 070, [[arXiv:1811.09593](#)].
- [20] A. von Manteuffel and L. Tancredi, *The two-loop helicity amplitudes for $gg \rightarrow V_1 V_2 \rightarrow 4$ leptons*, *JHEP* **06** (2015) 197, [[arXiv:1503.08835](#)].
- [21] F. Caola, J. M. Henn, K. Melnikov, A. V. Smirnov, and V. A. Smirnov, *Two-loop helicity amplitudes for the production of two off-shell electroweak bosons in gluon fusion*, *JHEP* **06** (2015) 129, [[arXiv:1503.08759](#)].
- [22] B. W. Lee, C. Quigg, and H. Thacker, *Weak Interactions at Very High-Energies: The Role of the Higgs Boson Mass*, *Phys. Rev. D* **16** (1977) 1519.
- [23] M. S. Chanowitz and M. K. Gaillard, *The TeV Physics of Strongly Interacting W's and Z's*, *Nucl. Phys. B* **261** (1985) 379–431.
- [24] K. Melnikov and M. Dowling, *Production of two Z-bosons in gluon fusion in the heavy top quark approximation*, *Phys. Lett. B* **744** (2015) 43–47, [[arXiv:1503.01274](#)].
- [25] F. Caola, M. Dowling, K. Melnikov, R. Rötsch, and L. Tancredi, *QCD corrections to vector boson pair production in gluon fusion including interference effects with off-shell Higgs at the LHC*, *JHEP* **07** (2016) 087, [[arXiv:1605.04610](#)].
- [26] J. M. Campbell, R. K. Ellis, M. Czakon, and S. Kirchner, *Two loop correction to interference in $gg \rightarrow ZZ$* , *JHEP* **08** (2016) 011, [[arXiv:1605.01380](#)].
- [27] R. Gröber, A. Maier, and T. Rauh, *Top quark mass effects in $gg \rightarrow ZZ$ at two loops and off-shell Higgs interference*, *Phys. Rev. D* **100** (2019), no. 11 114013, [[arXiv:1908.04061](#)].
- [28] J. Davies, G. Mishima, M. Steinhauser, and D. Wellmann, *$gg \rightarrow ZZ$: analytic two-loop results for the low- and high-energy regions*, *JHEP* **04** (2020) 024, [[arXiv:2002.05558](#)].
- [29] S. Alioli, S. Ferrario Ravasio, J. M. Lindert, and R. Rötsch, *Four-lepton production in gluon fusion at NLO matched to parton showers*, *Eur. Phys. J. C* **81** (2021), no. 8 687, [[arXiv:2102.07783](#)].
- [30] L. Buonocore, G. Koole, D. Lombardi, L. Rottoli, M. Wiesemann, and G. Zanderighi, *ZZ production at n NNLO+PS with MiNNLO_{PS}* , *JHEP* **01** (2022) 072, [[arXiv:2108.05337](#)].
- [31] B. Agarwal, S. P. Jones, and A. von Manteuffel, *Two-loop helicity amplitudes for $gg \rightarrow ZZ$ with full top-quark mass effects*, *JHEP* **05** (2021) 256, [[arXiv:2011.15113](#)].
- [32] C. Brønnum-Hansen and C.-Y. Wang, *Top quark contribution to two-loop helicity amplitudes for Z boson pair production in gluon fusion*, [arXiv:2101.12095](#).
- [33] D. A. Dicus, C. Kao, and W. Repko, *Gluon Production of Gauge Bosons*, *Phys. Rev. D* **36** (1987) 1570.
- [34] E. W. N. Glover and J. J. van der Bij, *Z boson pair production via gluon fusion*, *Nucl. Phys. B* **321** (1989) 561–590.
- [35] C. Zecher, T. Matsuura, and J. van der Bij, *Leptonic signals from off-shell Z boson pairs at hadron colliders*, *Z. Phys. C* **64** (1994) 219–226, [[hep-ph/9404295](#)].
- [36] J. Gluza, K. Kajda, and D. A. Kosower, *Towards a Basis for Planar Two-Loop Integrals*, *Phys. Rev. D* **83** (2011) 045012, [[arXiv:1009.0472](#)].
- [37] R. M. Schabinger, *A New Algorithm For The Generation Of Unitarity-Compatible Integration By Parts Relations*, *JHEP* **01** (2012) 077, [[arXiv:1111.4220](#)].
- [38] H. Ita, *Two-loop Integrand Decomposition into Master Integrals and Surface Terms*, *Phys. Rev. D* **94** (2016), no. 11 116015, [[arXiv:1510.05626](#)].
- [39] K. J. Larsen and Y. Zhang, *Integration-by-parts reductions from unitarity cuts and algebraic geometry*, *Phys. Rev. D* **93** (2016), no. 4 041701, [[arXiv:1511.01071](#)].
- [40] J. Böhm, A. Georgoudis, K. J. Larsen, M. Schulze, and Y. Zhang, *Complete sets of logarithmic vector fields for integration-by-parts identities of Feynman integrals*, *Phys. Rev. D* **98** (2018), no. 2 025023, [[arXiv:1712.09737](#)].
- [41] A. von Manteuffel and R. M. Schabinger, *A novel approach to integration by parts reduction*, *Phys. Lett. B* **744** (2015) 101–104, [[arXiv:1406.4513](#)].
- [42] T. Peraro, *Scattering amplitudes over finite fields and multivariate functional reconstruction*, *JHEP* **12** (2016) 030, [[arXiv:1608.01902](#)].
- [43] S. Abreu, J. Dormans, F. Febres Cordero, H. Ita, B. Page, and V. Sotnikov, *Analytic Form of the Planar Two-Loop Five-Parton Scattering Amplitudes in QCD*, *JHEP* **05** (2019) 084, [[arXiv:1904.00945](#)].
- [44] J. Boehm, M. Wittmann, Z. Wu, Y. Xu, and Y. Zhang, *IBP reduction coefficients made simple*, [arXiv:2008.13194](#).
- [45] H. A. Chawdhry, M. Czakon, A. Mitov, and R. Poncelet, *Two-loop leading-color helicity amplitudes for three-photon production at the LHC*, [arXiv:2012.13553](#).
- [46] M. Heller and A. von Manteuffel, *Multivariate Apart: Generalized Partial Fractions*, [arXiv:2101.08283](#).
- [47] B. Agarwal, F. Buccioni, A. von Manteuffel, and L. Tancredi, *Two-loop leading colour QCD corrections to $q\bar{q} \rightarrow \gamma\gamma g$ and $qg \rightarrow \gamma\gamma q$* , *JHEP* **04** (2021) 201, [[arXiv:2102.01820](#)].
- [48] S. Borowka, G. Heinrich, S. Jahn, S. Jones, M. Kerner, and J. Schlenk, *A GPU compatible quasi-Monte Carlo*

- integrator interfaced to pySecDec, *Comput. Phys. Commun.* **240** (2019) 120–137, [[arXiv:1811.11720](#)].
- [49] G. Heinrich, S. Jahn, S. P. Jones, M. Kerner, F. Langer, V. Magerya, A. Pödlaru, J. Schlenk, and E. Villa, *Expansion by regions with pySecDec*, *Comput. Phys. Commun.* **273** (2022) 108267, [[arXiv:2108.10807](#)].
- [50] G. Heinrich, S. P. Jones, M. Kerner, V. Magerya, A. Olsson, and J. Schlenk, *Numerical scattering amplitudes with pySecDec*, *Comput. Phys. Commun.* **295** (2024) 108956, [[arXiv:2305.19768](#)].
- [51] T. Gehrmann, A. von Manteuffel, and L. Tancredi, *The two-loop helicity amplitudes for $q\bar{q}' \rightarrow V_1 V_2 \rightarrow 4$ leptons*, *JHEP* **09** (2015) 128, [[arXiv:1503.04812](#)].
- [52] J. Vollinga and S. Weinzierl, *Numerical evaluation of multiple polylogarithms*, *Comput. Phys. Commun.* **167** (2005) 177, [[hep-ph/0410259](#)].
- [53] C. W. Bauer, A. Frink, and R. Kreckel, *Introduction to the GiNaC framework for symbolic computation within the C++ programming language*, *J. Symb. Comput.* **33** (2002) 1, [[cs/0004015](#)].
- [54] C. Anastasiou, S. Beerli, S. Bucherer, A. Daleo, and Z. Kunszt, *Two-loop amplitudes and master integrals for the production of a Higgs boson via a massive quark and a scalar-quark loop*, *JHEP* **01** (2007) 082, [[hep-ph/0611236](#)].
- [55] G. P. Lepage, *A New Algorithm for Adaptive Multidimensional Integration*, *J. Comput. Phys.* **27** (1978) 192.
- [56] T. Hahn, *CUBA: A Library for multidimensional numerical integration*, *Comput. Phys. Commun.* **168** (2005) 78–95, [[hep-ph/0404043](#)].
- [57] S. Catani, L. Cieri, D. de Florian, G. Ferrera, and M. Grazzini, *Universality of transverse-momentum resummation and hard factors at the NNLO*, *Nucl. Phys. B* **881** (2014) 414–443, [[arXiv:1311.1654](#)].
- [58] S. Catani and M. H. Seymour, *A General algorithm for calculating jet cross-sections in NLO QCD*, *Nucl. Phys. B* **485** (1997) 291–419, [[hep-ph/9605323](#)]. [Erratum: *Nucl. Phys. B* 510, 503–504 (1998)].
- [59] S. Catani, *The Singular behavior of QCD amplitudes at two loop order*, *Phys. Lett. B* **427** (1998) 161–171, [[hep-ph/9802439](#)].
- [60] **GoSam** Collaboration, G. Cullen, N. Greiner, G. Heinrich, G. Luisoni, P. Mastrolia, G. Ossola, T. Reiter, and F. Tramontano, *Automated One-Loop Calculations with GoSam*, *Eur. Phys. J. C* **72** (2012) 1889, [[arXiv:1111.2034](#)].
- [61] **GoSam** Collaboration, G. Cullen et al., *GOSAM-2.0: a tool for automated one-loop calculations within the Standard Model and beyond*, *Eur. Phys. J. C* **74** (2014), no. 8 3001, [[arXiv:1404.7096](#)].
- [62] J. Alwall, R. Frederix, S. Frixione, V. Hirschi, F. Maltoni, O. Mattelaer, H. S. Shao, T. Stelzer, P. Torrielli, and M. Zaro, *The automated computation of tree-level and next-to-leading order differential cross sections, and their matching to parton shower simulations*, *JHEP* **07** (2014) 079, [[arXiv:1405.0301](#)].
- [63] R. Frederix, S. Frixione, V. Hirschi, D. Pagani, H. S. Shao, and M. Zaro, *The automation of next-to-leading order electroweak calculations*, *JHEP* **07** (2018) 185, [[arXiv:1804.10017](#)]. [Erratum: *JHEP* 11, 085 (2021)].
- [64] F. Buccioni, J.-N. Lang, J. M. Lindert, P. Maierhöfer, S. Pozzorini, H. Zhang, and M. F. Zoller, *OpenLoops 2*, *Eur. Phys. J. C* **79** (2019), no. 10 866, [[arXiv:1907.13071](#)].
- [65] A. Denner, S. Dittmaier, and L. Hofer, *Collier: a fortran-based Complex One-Loop Library in Extended Regularizations*, *Comput. Phys. Commun.* **212** (2017) 220–238, [[arXiv:1604.06792](#)].
- [66] G. Ossola, C. G. Papadopoulos, and R. Pittau, *CutTools: A Program implementing the OPP reduction method to compute one-loop amplitudes*, *JHEP* **03** (2008) 042, [[arXiv:0711.3596](#)].
- [67] A. van Hameren, *OneLoop: For the evaluation of one-loop scalar functions*, *Comput. Phys. Commun.* **182** (2011) 2427–2438, [[arXiv:1007.4716](#)].
- [68] P. Mastrolia, E. Mirabella, and T. Peraro, *Integrand reduction of one-loop scattering amplitudes through Laurent series expansion*, *JHEP* **06** (2012) 095, [[arXiv:1203.0291](#)]. [Erratum: *JHEP* 11, 128 (2012)].
- [69] T. Peraro, *Ninja: Automated Integrand Reduction via Laurent Expansion for One-Loop Amplitudes*, *Comput. Phys. Commun.* **185** (2014) 2771–2797, [[arXiv:1403.1229](#)].
- [70] G. J. van Oldenborgh and J. A. M. Vermaseren, *New Algorithms for One Loop Integrals*, *Z. Phys. C* **46** (1990) 425–438.
- [71] T. Hahn and M. Perez-Victoria, *Automatized one loop calculations in four-dimensions and D-dimensions*, *Comput. Phys. Commun.* **118** (1999) 153–165, [[hep-ph/9807565](#)].
- [72] T.-J. Hou et al., *New CTEQ global analysis of quantum chromodynamics with high-precision data from the LHC*, *Phys. Rev. D* **103** (2021), no. 1 014013, [[arXiv:1912.10053](#)].
- [73] A. Buckley, J. Ferrando, S. Lloyd, K. Nordström, B. Page, M. Rüfenacht, M. Schönherr, and G. Watt, *LHAPDF6: parton density access in the LHC precision era*, *Eur. Phys. J. C* **75** (2015) 132, [[arXiv:1412.7420](#)].
- [74] A. Azatov, C. Grojean, A. Paul, and E. Salvioni, *Resolving gluon fusion loops at current and future hadron colliders*, *JHEP* **09** (2016) 123, [[arXiv:1608.00977](#)].
- [75] Q.-H. Cao, B. Yan, C. Yuan, and Y. Zhang, *Probing $Zt\bar{t}$ couplings using Z boson polarization in ZZ production at hadron colliders*, *Phys. Rev. D* **102** (2020), no. 5 055010, [[arXiv:2004.02031](#)].
- [76] D. Binosi and L. Theussl, *JaxoDraw: A Graphical user interface for drawing Feynman diagrams*, *Comput. Phys. Commun.* **161** (2004) 76–86, [[hep-ph/0309015](#)].
- [77] J. A. M. Vermaseren, *Axodraw*, *Comput. Phys. Commun.* **83** (1994) 45–58.